

# Photothermal and adsorption effects of silver selenide nanoparticles modified by different surfactants in nursing care of cancer patients

Xingju Yang<sup>a†</sup>, Chen Wang<sup>b†</sup>, Xiaoxu Zhang<sup>c</sup>, Yue Wang<sup>c</sup>, Feng Gao<sup>d</sup>, Lixia Sun<sup>a</sup>, Wenli Xu<sup>c</sup>, Changxiu Qiao<sup>e</sup> and Guiqin Zhang<sup>a</sup>

<sup>a</sup>Department of Nursing, Jinan People's Hospital Affiliated to Shandong First Medical University, Jinan China;

<sup>b</sup>Neurointerventional Department, The First Affiliated Hospital of Zhengzhou University, Zhengzhou, China;

<sup>c</sup>The Intensive Care Unit (ICU), Jinan People's Hospital Affiliated to Shandong First Medical University, Jinan China;

<sup>d</sup>Tumor Department, Jinan People's Hospital Affiliated to Shandong First Medical University, Jinan China;

<sup>e</sup>Nursing School of Binzhou Medical University, Binzhou, China

## ABSTRACT

Silver selenide nanoparticles have advantages of low cytotoxicity, desirable near-infrared light response characteristics, and easy surface modification, which attract increasing attention in chemo-photothermal therapy and nursing care of cancer patients. In this contribution, we synthesized Ag<sub>2</sub>Se nanoparticles modified by the surfactant of cetyltrimethylammonium bromide (CTAB) using a ligand exchange strategy. Their microstructure and composition were characterized by transmission electron microscopy, X-ray diffraction, X-ray Photo-electronic Spectroscopy, and Fourier transform infrared spectroscopy. The CTAB modified Ag<sub>2</sub>Se nanoparticles exhibited a uniform diameter distribution centered at ~12 nm. In order to investigate the photothermal and adsorption effects of CTAB-Ag<sub>2</sub>Se nanocomposites, we also prepared sodium dodecyl benzene sulfonate (SDBS) modified Ag<sub>2</sub>Se nanoparticles to make a comparison. The CTAB-Ag<sub>2</sub>Se nanoparticles showed high photothermal properties, a photothermal conversion efficiency of 20.1% and a high drug adsorption performance of 48.2 μg/mg. Importantly, the CTAB-Ag<sub>2</sub>Se-DOX presented an MCF-7 cell activity of only 27.3% under near-infrared radiation. The results revealed that the surface-modified Ag<sub>2</sub>Se nanoparticles with CTAB had stronger antitumor ability.

## ARTICLE HISTORY

Received 1 June 2020

Revised 20 July 2020

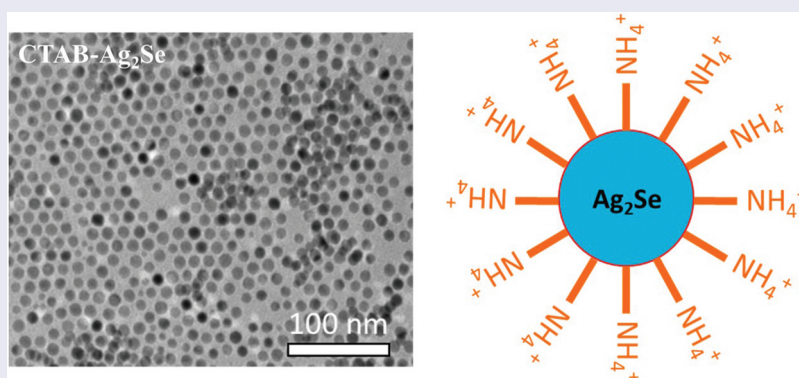
Accepted 21 July 2020

## KEYWORDS

Synthesis; characterization; photothermal; silver selenide; surfactants

## CLASSIFICATION

212 Surface and interfaces; 503 TEM; STEM; SEM; 301 Chemical syntheses / processing







## 1. Introduction


In recent years, photothermal therapy (PTT) has received widespread attention as an emerging therapy in cancer treatment, which uses the photothermal properties of photosensitive materials to trigger tumor cell ablation [1,2]. Nanomaterials for PTT are divided into two categories: organic and inorganic. Traditional organic compounds are indocyanine green, polyaniline, etc. [3–5]. Their disadvantages are low light-to-heat conversion rate and severe photobleaching. Inorganic photothermal

materials are based on noble metal nanoparticles [6–8]. The high price of noble metals stimulates the search for cheaper alternatives.

Metal selenides have recently attracted increasing attention because of their excellent optical properties, easiness in surface-functionalization and stability; therefore, they have been widely used in photocatalysis, optoelectronics, and energy storage [9–13]. Particularly, silver selenide possesses good biocompatibility and high efficiency in converting light to heat, making it a promising material in photothermal therapy of cancer patients [14–

**CONTACT** Guiqin Zhang  [guiqinzhang12@163.com](mailto:guiqinzhang12@163.com)  Department of Nursing, Jinan People's Hospital Affiliated to Shandong First Medical University, Jinan 271199, China; Changxiu Qiao  [changxiu-qiao@163.com](mailto:changxiu-qiao@163.com)  Nursing School of Binzhou Medical University, Binzhou 256603, China

<sup>†</sup>These authors equally contributed to this work.

 Supplemental data for this article can be accessed [here](#).

© 2020 The Author(s). Published by National Institute for Materials Science in partnership with Taylor & Francis Group.

This is an Open Access article distributed under the terms of the Creative Commons Attribution License (<http://creativecommons.org/licenses/by/4.0/>), which permits unrestricted use, distribution, and reproduction in any medium, provided the original work is properly cited.

16]. However, there are several issues that need to be concerned for cancer treatment based on PTT. Firstly, the insufficient light penetration depth may lead to incomplete elimination of cancer cells, which is the main hidden danger of thorough cancer treatment [17,18]. Secondly, the dispersibility of nanomaterials is also a problem to be solved [1,19]. Last but not least, the shortcomings of monotherapy cannot be ignored, current antitumor research tends to favor multiple approaches [20,21]. The combination of photothermal and chemotherapy can solve the hidden danger of recurrence in single PTT, and it is necessary to use photosensitive materials to explore more comprehensive treatment methods [22]. Recently, Li et al. prepared the Ag<sub>2</sub>Se quantum dots by the introduction of bovine serum albumin (BSA) as dispersant [23]. The Ag<sub>2</sub>Se@BSA composite showed good dispersibility, high biocompatibility and remarkable photothermal conversion. However, the drug delivery and photothermal therapy of Ag<sub>2</sub>Se@BSA need to for further combine with the extra mesoporous silica nanoparticles.

In this study, we reported the facile synthesis of Ag<sub>2</sub>Se nanoparticles modified by different surfactants including cetyltrimethylammonium bromide (CTAB), and sodium dodecyl benzene sulfonate (SDBS). Importantly, the CTAB-Ag<sub>2</sub>Se composite demonstrated improved antitumor ability. The CTAB as a surfactant can not only enhance the dispersive ability and biocompatibility of Ag<sub>2</sub>Se nanomaterials but also provide a porous layer on the Ag<sub>2</sub>Se surface to achieve higher drug loading capacity. At the same time, due to the excellent photothermal performance of Ag<sub>2</sub>Se nanoparticles, this strategy can achieve the expected purpose.

## 2. Experimental section

### 2.1 Materials

All chemical reagents were used without further purification. Dodecanethiol (98%), CTAB, SDBS, concentrated HCl (37%), ethanol, doxorubicinhydrochloride (DOX·HCl), and dimethyl sulfoxide (DMSO) were purchased from Aladdin Chemical Inc. (Shanghai, China). Michigan cancer foundation-7 (MCF-7) cells were obtained from the Jinan City People's Hospital. The 3-(4,5-dimethyl-2-thiazolyl)-2-5-diphenyl-2 H-tetrazolium-bromide (MTT) was purchased from Shanghai Pumai Biotechnology.

### 2.2 Synthesis of CTAB and SDBS modified Ag<sub>2</sub>Se nanoparticles

The oil-soluble dodecanethiol modified Ag<sub>2</sub>Se nanoparticles were synthesized according to a reported study [24]. CTAB and SDBS modified Ag<sub>2</sub>Se nanoparticles were prepared using the ligand exchange strategy on the basis of above dodecanethiol-Ag<sub>2</sub>Se

nanoparticles. Detailedly, 100 mg dodecanethiol-Ag<sub>2</sub>Se precursors were dissolved in 20 ml chloroform and 20 ml H<sub>2</sub>O, followed by addition with 4 g CTAB. The mixtures were kept at 50°C under the N<sub>2</sub> protection and stirred for 4 h. After cooling down to room temperature, the products were collected and washed with ethanol and re-dispersing in distilled water. Similarly, the SDBS-Ag<sub>2</sub>Se nanoparticles were obtained by replacing dodecanethiol ligand with SDBS. Briefly, 100 mg dodecanethiol-Ag<sub>2</sub>Se precursors and 4 g SDBS were dispersed in 40 ml chloroform, which was then refluxed at 60°C under the N<sub>2</sub> protection and stirred for 12 h. After the reaction, the collected samples were washed with chloroform and ethanol and re-dispersing in distilled water.

### 2.3 Characterization

The morphology of the prepared samples was characterized by transmission electron microscopy (TEM; JEM 2100, Jeol, Tokyo, Japan), and elemental mapping images were obtained using energy dispersive spectroscopy (EDS). The phase compositions of the samples were determined by X-ray diffraction (XRD; D/max-2500, Cu K $\alpha$ ). Fourier transform infrared (FTIR) spectra were recorded with a model-8400s FTIR spectrometer (Shimadzu, Japan). N<sub>2</sub> adsorption-desorption isotherms were obtained using a Builder SSA-4200 instrument at 77 K. X-ray photoelectron spectroscopy (XPS) spectra were recorded by a PHI5600X of PerkinElmer from USA. A 980 nm diode laser was obtained from Changchun New Industries Optoelectronics Technology Co. Ltd. (Jilin, China).

### 2.4 Measurement of the photothermal effect

To measure the photothermal performance, sample nanoparticles were dispersed in deionized water with different concentrations (0, 0.0625, 0.125, 0.25, 0.5 and 1 mg/mL). To evaluate the photothermal performance, 2 mL of deionized water, CTAB-Ag<sub>2</sub>Se and SDBS-Ag<sub>2</sub>Se aqueous dispersions with different concentrations were irradiated for 10 min by an external adjustable power (0–1.66 W/cm<sup>2</sup>) 980 nm semiconductor laser device. The output power was independently calibrated using an optical power meter. The temperature evolution of the aqueous dispersions under irradiation was recorded by using a hand-held thermometer every 2 min. To measure the photothermal conversion efficiency ( $\eta$ ), the temperature change of the CTAB-Ag<sub>2</sub>Se and SDBS-Ag<sub>2</sub>Se dispersions were recorded as a function of time under continuous irradiation of the 980 nm laser with a power density of 1.66 W/cm<sup>2</sup> until the solution reached a steady-state temperature. The  $\eta$  value was calculated by eq (1) [25]:

$$\eta = \frac{hS(T_m - T_s) - Q_s}{I(1 - 10^{-A_\lambda})} \quad (1)$$

where  $h$  is the heat transfer coefficient,  $S$  is the surface area of the container,  $T_m$  is the equilibrium temperature,  $T_s$  is the ambient temperature of the surroundings,  $Q_s$  stands for the heat input due to the absorption of water,  $I$  is the incident laser power, and  $A_\lambda$  is the absorbance of the cesium tungsten bronze nanomaterial at 980 nm [26].

### 2.5 Loading and release of DOX

Firstly, 1.0 mg of CTAB-Ag<sub>2</sub>Se and SDBS-Ag<sub>2</sub>Se nanoparticles were dispersed into DOX phosphate-buffered saline (PBS) solution (5.0 mL, 1 mg/mL). Next, the DOX-loaded samples were centrifuged at 8000 rpm and then washed repeatedly with PBS solution to remove free DOX molecules. All the washing solutions were collected and measured by a UV-vis spectrophotometer. The measurements were performed in triplicate, and the loading amount of DOX was calculated using eq. (2).

$$\text{Drug loading capacity} = \frac{M_{DOX}}{M_{NPs} + M_{DOX}} \quad (2)$$

where  $M_{DOX}$  is the mass of DOX,  $M_{NPs}$  is the mass of CTAB-Ag<sub>2</sub>Se nanoparticles. The unit of drug loading capacity is  $\mu\text{g}/\text{mg}$ . The release behavior of DOX was studied in PBS solution (pH 7.4 and pH 5.0) at room temperature. DOX-loaded CTAB-Ag<sub>2</sub>Se and SDBS-Ag<sub>2</sub>Se nanocomposites were dispersed in 30 mL of PBS solution and stirred. The supernatants were centrifuged every several hours to measure the released DOX and then replaced with fresh PBS solution. All the tests were carried out in triplicate and the average values are reported.

### 2.6 In vitro cell toxicity assay

The cytotoxicity of CTAB-Ag<sub>2</sub>Se nanocomposites was evaluated by a standard MTT assay using MCF-7 cells as models. MCF-7 cells were inoculated in 96-well plate at 104/well for 6 groups. Five parallels for each group were conducted. CTAB-Ag<sub>2</sub>Se suspensions (0, 0.0625, 0.125, 0.25, 0.5, and 1 mg/mL) were added to the cells. After incubating for 24 h, the medium was then aspirated using a pipette and fresh medium was added to the culture dishes. Next, the cancer cells were irradiated with a 980 nm near-infrared (NIR) laser for 5 minutes, washed gently with PBS three times to wash away the nanomaterials that were not phagocytized by the cells, then placed in an incubator for further 4 hours. Subsequently, 20  $\mu\text{L}$  MTT solutions (5 mg/mL) were injected and maintained for 4 h after incubation. Then, the medium was removed and 150  $\mu\text{L}$  DMSO was injected. After shaking the plate for 15 min, the

absorbance was measured at 490 nm to calculate the cell survival rate.

## 3. Results and discussion

The morphology of the as-prepared CTAB-Ag<sub>2</sub>Se nanoparticles has been studied by TEM technique, as shown in Figure 1(a). These particles possess excellent dispersion and uniform distribution in a diameter of around 12 nm (Figure 1(b)). The amine salt type cationic surfactant of CTAB is able to effectively restrain the intergranular agglomeration through the surface modification for Ag<sub>2</sub>Se nanoparticles. Figure 1(c) displays the high-resolution TEM image of CTAB-Ag<sub>2</sub>Se nanoparticles, we can observe a group of well-resolved lattice fringe with the interplanar distance of 0.24 nm, it is ascribed to the (0 1 3) plane of the orthorhombic phase of Ag<sub>2</sub>Se [27]. The EDX spectrum in Figure 1(d) presents the signals from element N, Ag, and Se, indicative of the successful preparation of CTAB-Ag<sub>2</sub>Se nanocomposites. The peak at 2.2 keV is the Au signal, which has been used to improve the conductivity of the sample. The schematic diagram of such a composite nanoparticle is depicted in Figure 1(e) where Ag<sub>2</sub>Se nanoparticle is covered by a layer of CTAB with the exposed NH<sub>4</sub><sup>+</sup> group. The structural information of CTAB-Ag<sub>2</sub>Se nanoparticles can be further obtained from elemental mapping results in Figure 1(f). The Ag, Se, and N elements demonstrate the homogeneous distributions over the nanoparticles, confirming the above results. For comparison, the anionic surfactant SDBS modified Ag<sub>2</sub>Se nanoparticles have been also synthesized, and Fig. S1 gives their TEM image and schematic diagram.

XPS analysis has been employed to study the chemical composition and oxidation states of prepared material. As shown in Figure 2(a), the higher binding energies (compared to Ag(0)) located at 367.9 eV and 374.2 eV stand for Ag 3d<sub>5/2</sub> and Ag 3d<sub>3/2</sub>, respectively, indicating the presence of oxidized Ag(I) species in Ag<sub>2</sub>Se [28]. The band situated at 54.2 eV in Figure 2(b) is assigned to Se 3d containing two contributions from Se 3d<sub>5/2</sub> and Se 3d<sub>3/2</sub>, which agrees well with the reported result of Ag<sub>2</sub>Se nanomaterial [29].

The FTIR spectra in Figure 3(a) confirm the surface modification of Ag<sub>2</sub>Se nanoparticles by CTAB and SDBS surfactants. The three obvious peaks at 2910 cm<sup>-1</sup>, 2843 cm<sup>-1</sup>, and 1467 cm<sup>-1</sup> are characteristic signals of 1-dodecanethiol. Compared to the pure Ag<sub>2</sub>Se, the distinctive peaks at 1407 cm<sup>-1</sup> and 1693 cm<sup>-1</sup> of SDBS-Ag<sub>2</sub>Se sample correspond to the symmetric and asymmetric COO<sup>-</sup> stretching modes [30], indicating that SDBS exists on the surface of Ag<sub>2</sub>Se nanoparticles. In the spectrum of CTAB-Ag<sub>2</sub>Se sample, we can observe several characteristic peaks located at 3035 cm<sup>-1</sup>, 1484 cm<sup>-1</sup>, and 1589 cm<sup>-1</sup>, they are ascribed to the NH<sub>4</sub><sup>+</sup> stretching vibration, NH<sub>4</sub><sup>+</sup> deformation vibration, and the N-H

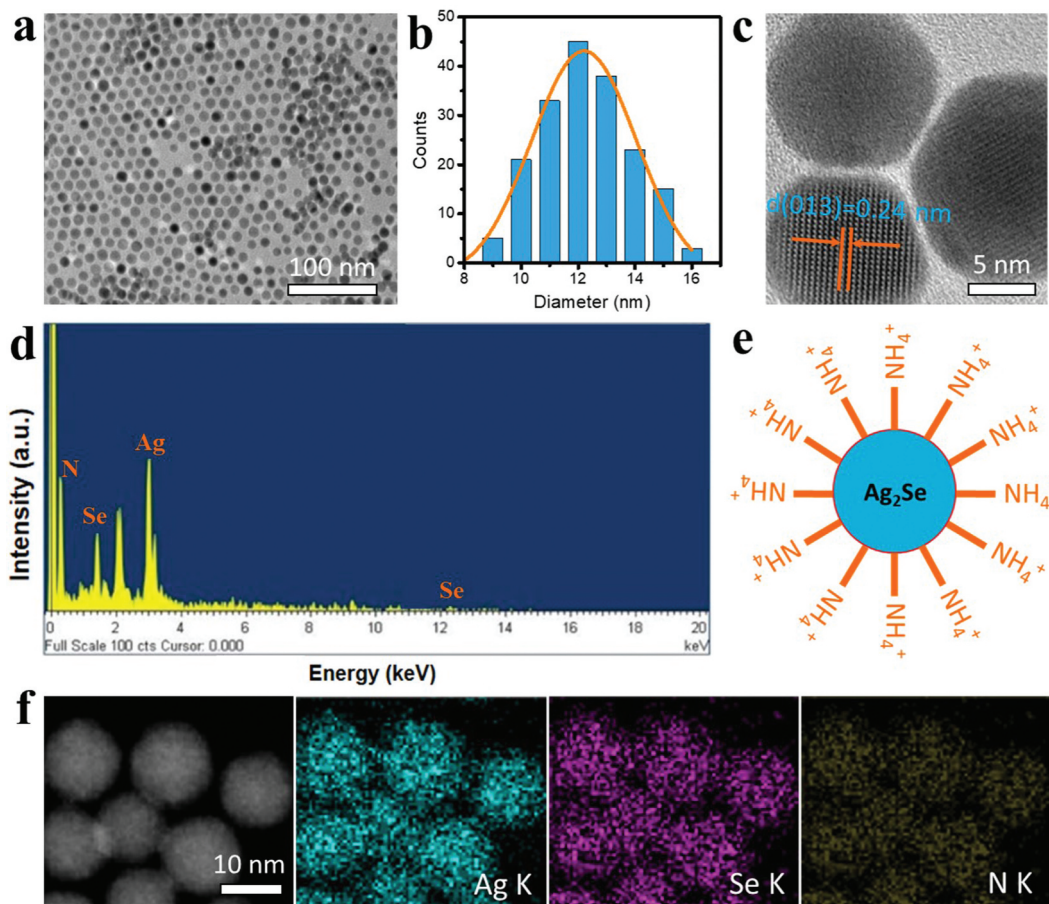


**Figure 1.** TEM image (a), diameter distribution (b), high-resolution TEM image (c), and EDS spectrum (d) of CTAB-Ag<sub>2</sub>Se nanoparticles. (e) Illustration of CTAB-Ag<sub>2</sub>Se nanoparticles with exposed NH<sub>4</sub><sup>+</sup> group. (f) elemental maps of CTAB-Ag<sub>2</sub>Se nanoparticles.

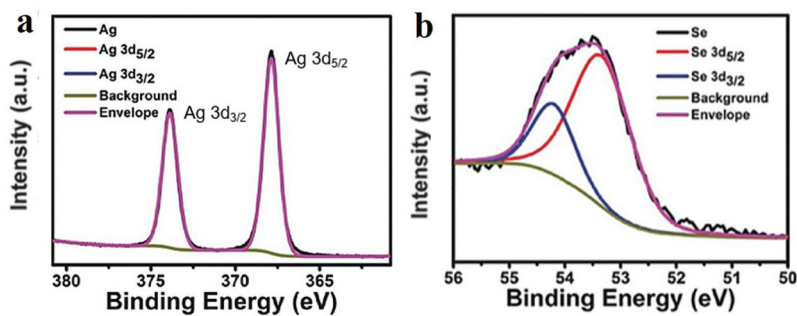


**Figure 2.** XPS spectra of the as-prepared Ag<sub>2</sub>Se nanoparticles around the Ag 3d (a) and Se 3d (b) edges.

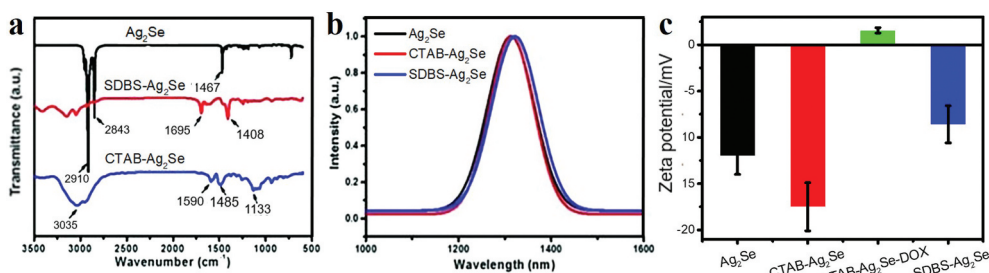


**Figure 3.** FTIR transmittance (a), spectra are vertically offset for clarity, photoluminescence emission spectra (b), and zeta potentials (c) of Ag<sub>2</sub>Se, CTAB-Ag<sub>2</sub>Se, and SDBS-Ag<sub>2</sub>Se nanoparticles.

bending vibration, respectively [31]. Both CTAB-Ag<sub>2</sub>Se and SDBS-Ag<sub>2</sub>Se nanocomposites retain the NIR II fluorescence properties of Ag<sub>2</sub>Se nanoparticles (Figure 3(b)), their emission wavelengths are around 1320 nm. The zeta potentials of Ag<sub>2</sub>Se, CTAB-Ag<sub>2</sub>Se, and SDBS-Ag<sub>2</sub>Se nanoparticles have been recorded and provided in Figure 3(c). The zeta potential of CTAB-Ag<sub>2</sub>Se was about -12.13 mV, while it changed to 1.68 mV when DOX was installed. The change in charge of zeta potential further illustrated the load of DOX. However, the zeta potential of the SDBS-Ag<sub>2</sub>Se was only -8.04 mV, which indicated that the CTAB-Ag<sub>2</sub>Se had a better adsorption amount of DOX than that of SDBS-Ag<sub>2</sub>Se.

The photothermal performance of the samples is shown in Figure 4. The samples of CTAB-Ag<sub>2</sub>Se and SDBS-Ag<sub>2</sub>Se nanocomposites were dispersed in distilled water at different concentrations (0, 0.25, 0.5, and 1 mg/mL) to study the photothermal heating effect. Subsequently, they were irradiated by NIR 980 nm laser irradiation at a power density of 1.66 W cm<sup>-2</sup> for 20 min. As demonstrated in Figure 4(a, b), the temperature only slightly increased in distilled water, while obvious increases were observed in CTAB-Ag<sub>2</sub>Se and SDBS-Ag<sub>2</sub>Se. SDBS-Ag<sub>2</sub>Se is more responsive to temperature and the temperature can be controlled from 20.6°C to 56.8°C by adjusting the composite content. To further investigate the photothermal transduction ability (Figs. S2a, b), we evaluated the temperature changes of CTAB-Ag<sub>2</sub>Se and SDBS-Ag<sub>2</sub>Se suspension (1 mg/mL) under

different laser power densities of 980 nm continuous-wave lasers. The photothermal curve shows that the CTAB-Ag<sub>2</sub>Se and SDBS-Ag<sub>2</sub>Se also have the strong laser power-dependent photothermal effects. These results indicated that SDBS-Ag<sub>2</sub>Se nanocomposites could convert the energy of a 980 nm laser into heat more quickly and efficiently. Thermal properties are also very important for achieving high photothermal conversion. As can be seen intuitively from Figure 4(c) and Fig. S2c, obvious rapid temperature changes can be observed in the groups of SDBS-Ag<sub>2</sub>Se ( $\Delta T = 37^\circ\text{C}$ ) and CTAB-Ag<sub>2</sub>Se ( $\Delta T = 27^\circ\text{C}$ ) with the concentration of 1 mg/mL and a power density of 1.66 W/cm<sup>2</sup>. The results indicate that the Ag<sub>2</sub>Se nanoparticles modified by surfactants have concentration-dependent temperature elevations and excellent photothermal conversion. Therefore, we believe that SDBS-Ag<sub>2</sub>Se nanocomposites have the superior potential for photothermal therapy.

In order to further study its photothermal conversion efficiency, according to Figure 5(a, b), the photothermal conversion ability of the material has been evaluated by the photothermal conversion efficiency ( $\eta$ ). The dispersion liquid (2 ml, 0.5 mg/ml) has been irradiated with a 980 nm laser for 20 minutes, and then naturally cooled. Figure 5(b) shows the curve of cooling time  $t(-\ln\theta)$ , calculated according to the method in the literature [32], the photothermal conversion efficiencies of SDBS-Ag<sub>2</sub>Se and CTAB-Ag<sub>2</sub>Se are 22.9% and 20.1%, respectively. Anionic surfactant

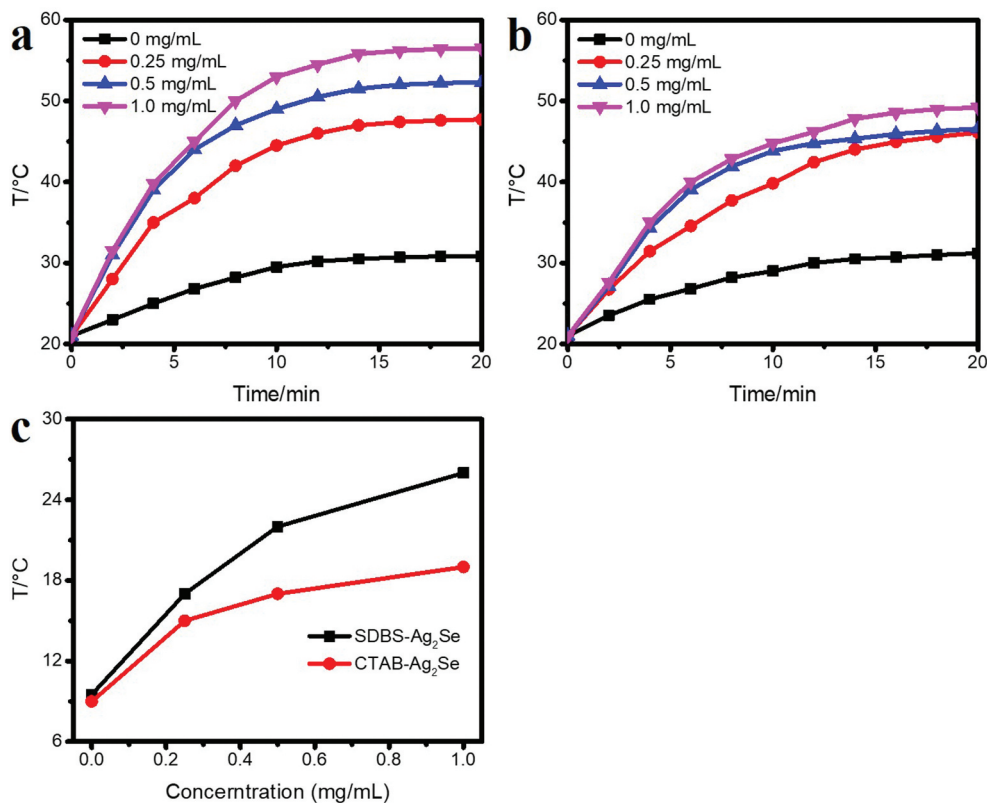


**Figure 4.** NIR-induced heat generation in SDBS-Ag<sub>2</sub>Se (a) and CTAB-Ag<sub>2</sub>Se (b) suspensions at different concentrations. (c) NIR-induced temperature increase for SDBS-Ag<sub>2</sub>Se and CTAB-Ag<sub>2</sub>Se at different concentrations.

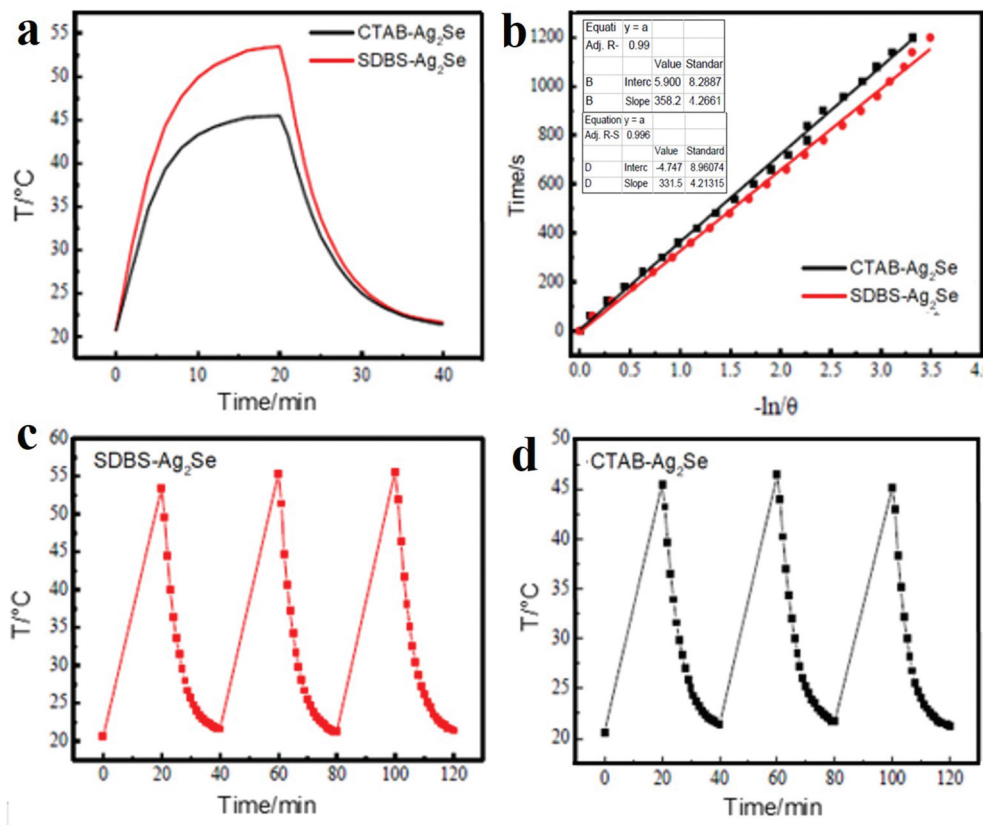


**Figure 5.** (a) The photothermal response of SDBS-Ag<sub>2</sub>Se aqueous dispersion (2 mL, 0.5 mg/mL) under a pulse of laser irradiation (1.66 W, 980 nm). (b) Plots of cooling time (after 20 min) versus negative natural logarithm of the driving force temperature (-ln/θ) obtained from cooling stage as shown in (a). SDBS-Ag<sub>2</sub>Se (c) and CTAB-Ag<sub>2</sub>Se (d) aqueous dispersion photothermal cycle diagram.

SDBS may have a larger influence on the electronic structure of the Ag<sub>2</sub>Se nanoparticles, thus leading to the superior photothermal property. As shown in Figure 5(c, d), the temperature changes of SDBS-Ag<sub>2</sub>Se and CTAB-Ag<sub>2</sub>Se dispersion liquid (0.5 mg/ml) have no obvious reduction after repeatedly turning on or off the laser for 3 times, implying that the colloidal SDBS-Ag<sub>2</sub>Se and CTAB-Ag<sub>2</sub>Se nanocomposites had excellent photothermal stability.

The SDBS-Ag<sub>2</sub>Se and CTAB-Ag<sub>2</sub>Se nanocomposites are promising candidates to use as drug delivery platforms for PTT based on their structural characteristics. Thus, the anticancer drug DOX has been used to evaluate the drug adsorption behaviors of both nanomaterial carriers. At the same concentration, the drug adsorption capacity of CTAB-Ag<sub>2</sub>Se is significantly higher than that of SDBS-Ag<sub>2</sub>Se. As shown in Figure 6(a), the drug loading capacity of CTAB-Ag<sub>2</sub>Se is 48.2 μg/mL while it is only 25.3 μg/mL for SDBS-Ag<sub>2</sub>Se with the concentration of 50 μg/mg. Figure 6(b) displays the adsorption capacity of SDBS-Ag<sub>2</sub>Se and CTAB-Ag<sub>2</sub>Se at the maximum concentration as the loading time changes, and the adsorption amount of the sample gradually increases and tends to the absorption equilibrium. It is clear that CTAB-Ag<sub>2</sub>Se has the excellent adsorption ability. The reason may be due to its porous structure (larger pore diameter of 0.9–1.1 nm for CTAB-Ag<sub>2</sub>Se than 0.7–0.8 nm for

SDBS-Ag<sub>2</sub>Se, as shown in Fig. S3) which was formed by treatment the sample with a certain ratio of methanol-hydrochloric acid reflux. The drug release behavior of CTAB-Ag<sub>2</sub>Se-DOX has been used to investigate the efficacy of chemotherapy in cancer treatment. For this, pH 7.4 PBS with or without near-infrared light and pH 5.0 PBS are used to mimic normal tissues and the microenvironments of tumor tissues with or without NIR light, respectively. Figure 6(c) shows the cumulative DOX release from the CTAB-Ag<sub>2</sub>Se-DOX under different conditions. The percentage cumulative drug release of CTAB-Ag<sub>2</sub>Se could reach up to 44.63% under pH 5.0, which was higher than that under pH 7.4. The release of this drug may be due to the weakening of the electrostatic interaction between DOX and CTAB-Ag<sub>2</sub>Se nanoparticles. Moreover, it is clearly seen that the behavior of DOX releasing has been enhanced under the irradiation, and the cumulative drug release in pH 5 and 7 are 49.16% and 48.31%, respectively. The drug release efficiencies are comparable to the reported results, such as mesoporous silica nanoparticles, nanoporous gold wires, and bovine serum albumin modified Ag<sub>2</sub>Se quantum dots [23,33,34]. It can be attributed to the fact that the Ag<sub>2</sub>Se nanomaterial effectively converts the infrared laser energy into heat, which weakens the interaction force between

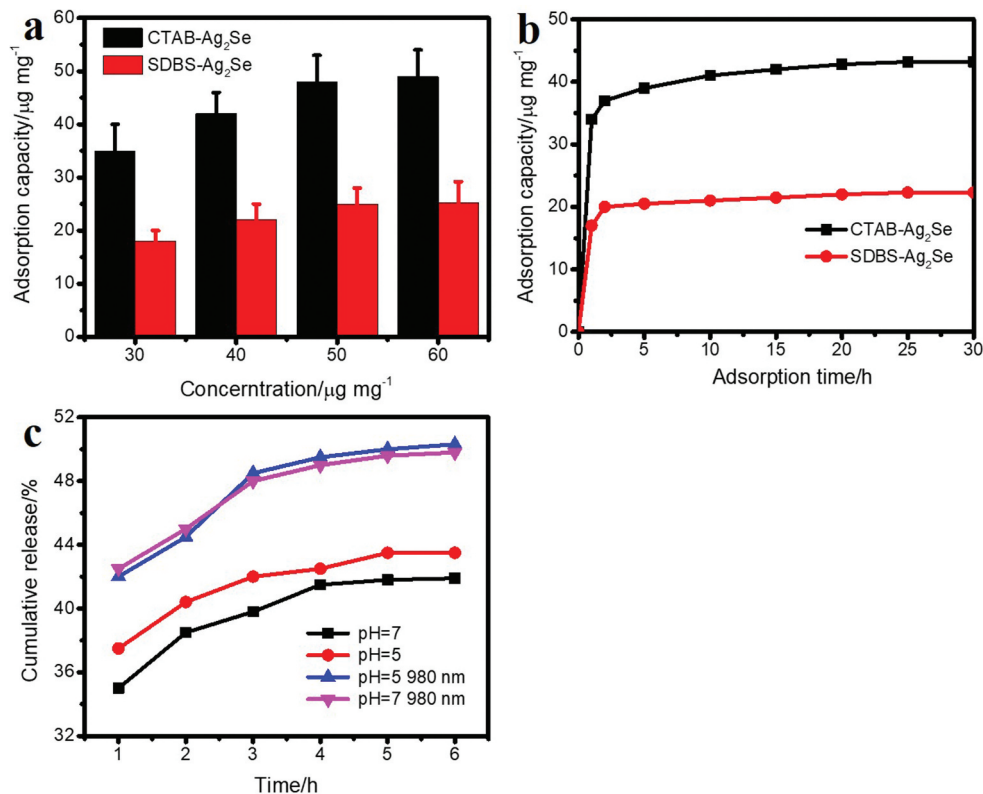


**Figure 6.** (a) Adsorption capacity of CTAB- $\text{Ag}_2\text{Se}$  and SDBS- $\text{Ag}_2\text{Se}$  nanoparticles at different concentrations. (b) The adsorption amount of the sample at the maximum concentration with time. (c) Drug release profiles of CTAB- $\text{Ag}_2\text{Se}$  in pH 7 and pH 5.0 PBS within 6 h.

the drug and the nanomaterial, and thus helps the drug release.

The CTAB- $\text{Ag}_2\text{Se}$  carrier has been chosen to evaluate the cytotoxicity towards MCF-7 cells based on its prominent photothermal effect and high drug adsorption efficiency. According to Figure 7(a), the viabilities of MCF-7 cells incubated with blank CTAB- $\text{Ag}_2\text{Se}$  nanoparticles at a high concentration of 1 mg/mL were above 80%, suggesting the high safety in the absence of NIR. Free DOX showed concentration-dependent toxicity to MCF-7 cells. In addition, when the concentration range is 0–1 mg/mL without NIR laser, CTAB- $\text{Ag}_2\text{Se}$  has

been used as a drug carrier, and the cell activity decreased significantly with increasing concentration, from 83% to 66%, indicating that the anti-tumor efficiency of DOX released by nanocomposites was comparable to that of free DOX. To evaluate the effect, cells were irradiated with 980 nm laser, CTAB- $\text{Ag}_2\text{Se}$  and CTAB- $\text{Ag}_2\text{Se}$ -DOX were subjected to NIR laser at a power density of 1.66 W/cm<sup>2</sup> under specific conditions. As shown in Figure 7(b), in the near-infrared irradiation group, the cell viability in the range of 0–1 mg/mL DOX is much lower than that of the free DOX without light, suggesting that the near-infrared laser irradiation

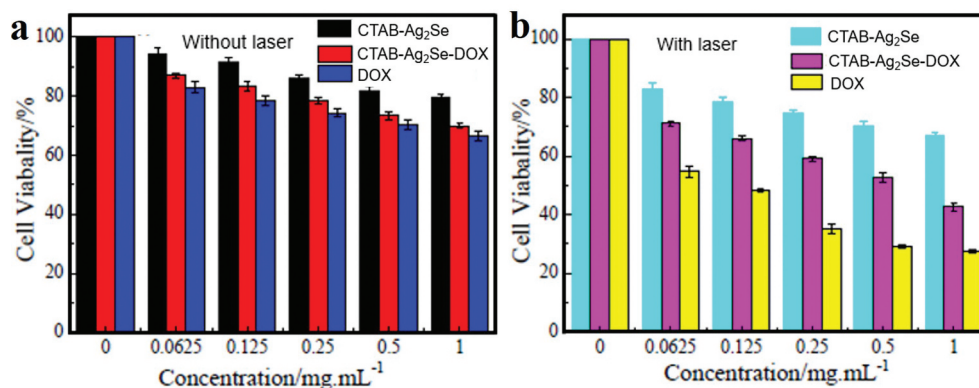


**Figure 7.** Viability of MCF-7 cells incubated with the control group and different concentrations of DOX, CTAB- $\text{Ag}_2\text{Se}$ , CTAB- $\text{Ag}_2\text{Se}$ -DOX without (a) and with (b) irradiation.

has a significant effect on MCF-7 cell viability. However, for CTAB-Ag<sub>2</sub>Se with NIR radiation, an increase in the cytotoxicity of MCF-7 cells has been observed with increasing concentration of CTAB-Ag<sub>2</sub>Se, confirming that CTAB-Ag<sub>2</sub>Se can effectively absorb near-infrared light and convert it into thermal energy to induce MCF-7 cell apoptosis. For CTAB-Ag<sub>2</sub>Se-DOX with near-infrared radiation, more pronounced cytotoxicity is produced, and the cell activity is only 27.3% when the concentration of CTAB-Ag<sub>2</sub>Se-DOX is 1 mg/ml.

#### 4. Conclusions

In summary, we have synthesized CTAB modified Ag<sub>2</sub>Se nanoparticles with low toxicity and improved antitumor ability by a ligand exchange method. TEM results show that the prepared CTAB-Ag<sub>2</sub>Se nanoparticles have a uniform diameter distribution centered at 12 nm. The CTAB layer enhances the dispersive ability and biocompatibility of Ag<sub>2</sub>Se nanomaterials, and also improves the drug loading capacity. The CTAB-Ag<sub>2</sub>Se nanocomposite exhibits a drug adsorption capacity of 48.2 µg/mg, which is much higher than that of SDBS-Ag<sub>2</sub>Se (25.3 µg/mg). Cytotoxicity tests demonstrated that CTAB-Ag<sub>2</sub>Se with high drug load had a stronger therapeutic effect. Hence, suitable surface modifiers have potential application value for photothermal nanomaterials in combination therapy, providing additional possibilities for future research on clinical therapeutic materials.

#### Disclosure statement

The authors declare no conflicts of interest.

#### References

- [1] Lal S, Clare SE, Halas NJ. Nanoshell-enabled photothermal cancer therapy: impending clinical impact. *Acc Chem Res.* 2008;41(12):1842–1851.
- [2] Zhang X, Wang L, Wu X, et al. Synthesis of SiO<sub>2</sub>@Cu<sub>2-x</sub>Se nanospheres for efficient near-infrared radiation mediated treatment and care of gastric cancer patients. *J Photoch Photobio B.* 2020;206:111849–111857.
- [3] Zheng M, Yue C, Ma Y, et al. Single-step assembly of DOX/ICG loaded lipid-polymer nanoparticles for highly effective chemo-photothermal combination therapy. *ACS Nano.* 2013;7:2056–2067.
- [4] Sheng Z, Hu D, Zheng M, et al. Smart human serum albumin-indocyanine green nanoparticles generated by programmed assembly for dual-modal imaging-guided cancer synergistic phototherapy. *ACS Nano.* 2014;8(12):12310–12322.
- [5] Zhou J, Lu Z, Zhu X, et al. NIR photothermal therapy using polyaniline nanoparticles. *Biomater.* 2013;34(37):9584–9592.
- [6] Dykman LA, Khlebtsov NG. Gold nanoparticles in biomedical applications: recent advances and perspectives. *Chem Soc Rev.* 2012;41:2256–2282.
- [7] Boca S, Potara M, Gabudean A, et al. Chitosan-coated triangular silver nanoparticles as a novel class of biocompatible, highly effective photothermal transducers for in vitro cancer cell therapy. *Cancer Lett.* 2011;311:131–140.
- [8] Cheng X, Sun R, Yin L, et al. Light-triggered assembly of gold nanoparticles for photothermal therapy and photoacoustic imaging of tumors in vivo. *Adv Mater.* 2017;29(6):1604894–1604899.
- [9] Zhu L, Ye S, Ali A, et al. Modified hydrothermal synthesis and characterization of reduced graphene oxide-silver selenide nanocomposites with enhanced reactive oxygen species generation. *Chin J Catal.* 2015;36(4):603–611.
- [10] Eftekhari A. Molybdenum diselenide (MoSe<sub>2</sub>) for energy storage, catalysis, and optoelectronics. *Appl Mater Today.* 2017;8:1–17.
- [11] Wang Z, Yue HY, Yu ZM, et al. One-pot hydrothermal synthesis of MoSe<sub>2</sub> nanosheets spheres-reduced graphene oxide composites and application for high-performance supercapacitor. *J Mater Sci: Mater Electron.* 2019;30:8537–8545.
- [12] Meng Z, Zhu L, Ghosh T, et al. Ag<sub>2</sub>Se-graphene/TiO<sub>2</sub> nanocomposites, sonochemical synthesis and enhanced photocatalytic properties under visible light. *Bull Korean Chem Soc.* 2012;33:3761–3766.
- [13] Cao H, Xiao Y, Lu Y, et al. Ag<sub>2</sub>Se complex nanostructures with photocatalytic activity and superhydrophobicity. *Nano Res.* 2010;3(12):863–873.
- [14] Cui R, Gu Y, Bao L, et al. Near-infrared electrogenerated chemiluminescence of ultrasmall Ag<sub>2</sub>Se quantum dots for the detection of dopamine. *Anal Chem.* 2012;84(21):8932–8935.
- [15] Zhu C, Chen G, Tian Z, et al. Near-Infrared fluorescent Ag<sub>2</sub>Se-cetuximab nanoprobe for targeted imaging and therapy of cancer. *Small.* 2017;13(3):1602309–1602318.
- [16] Du K, Lei P, Dong L, et al. In situ decorating of ultrasmall Ag<sub>2</sub>Se on upconversion nanoparticles as novel nanotheranostic agent for multimodal imaging-guided cancer photothermal therapy. *Appl Mater Today.* 2020;18:100497–100511.
- [17] Liu Y, Bhattarai P, Dai Z, et al. Photothermal therapy and photoacoustic imaging via nanotheranostics in fighting cancer. *Chem Soc Rev.* 2019;48:2053–2108.
- [18] Yang K, Zhang S, Zhang G, et al. Graphene in mice: ultrahigh in vivo tumor uptake and efficient photothermal therapy. *Nano Lett.* 2010;10(9):3318–3323.
- [19] Li J, Rao J, Pu K. Recent progress on semiconducting polymer nanoparticles for molecular imaging and cancer phototherapy. *Biomater.* 2018;155:217–235.
- [20] Gai S, Yang G, Yang P, et al. Recent advances in functional nanomaterials for light-triggered cancer therapy. *Nano Today.* 2018;19:146–187.
- [21] Zhen X, Xie C, Pu K. Temperature-correlated afterglow of a semiconducting polymer nanococktail for imaging-guided photothermal therapy. *Angew Chem Int Ed.* 2018;130:4002–4006.
- [22] Wang J, Dong Y, Li Y, et al. Designer exosomes for active targeted chemo-photothermal synergistic tumor therapy. *Adv Funct Mater.* 2018;28(18):1707360–1707373.
- [23] Li X, Liu Z, Luo K, et al. Biomimetic synthesis of Ag<sub>2</sub>Se quantum dots with enhanced photothermal



- properties and as “gatekeepers” to cap mesoporous silica nanoparticles for chemo-photothermal therapy. *Chem Asian J.* **2019**;14(1):155–161.
- [24] Dong BH, Li CY, Chen GC, et al. Facile synthesis of highly photoluminescent  $\text{Ag}_2\text{Se}$  quantum dots as a new fluorescent probe in the second near-infrared window for in vivo imaging. *Chem Mater.* **2013**;25(12):2503–2509.
- [25] Lei Z, Zhang W, Li B, et al. A full-spectrum-absorption from nickel sulphide nanoparticles for efficient NIR-II window photothermal therapy. *Nanoscale.* **2019**;11:20161–20170.
- [26] Miao ZH, Wang H, Yang H, et al. Glucose-derived carbonaceous nanospheres for photoacoustic imaging and photothermal therapy. *ACS Appl Mater Interfaces.* **2016**;8(25):15904–15910.
- [27] Wang J, Fan W, Yang J, et al. Tetragonal–Orthorhombic–Cubic phase transitions in  $\text{Ag}_2\text{Se}$  nanocrystals. *Chem Mater.* **2014**;26(19):5647–5653.
- [28] Yu H, Liu W, Wang X, et al. Promoting the interfacial  $\text{H}_2$ -evolution reaction of metallic Ag by  $\text{Ag}_2\text{S}$  cocatalyst: a case study of  $\text{TiO}_2/\text{Ag}-\text{Ag}_2\text{S}$  photocatalyst. *Appl Catal B-Environ.* **2018**;225:415–423.
- [29] Gong J, Tian Y, Yang Z, et al. High-performance flexible all-solid-state asymmetric supercapacitors based on vertically aligned  $\text{CuSe}@\text{Co}(\text{OH})_2$  nanosheet arrays. *J Phys Chem C.* **2018**;122(4):2002–2011.
- [30] Ibrahim M, Nada A, Kamal DE. Density functional theory and FTIR spectroscopic study of carboxyl group. *Indian J Pure Ap Phy.* **2005**;43:911–917.
- [31] De Waal D, Heyns AM, Range KJ, et al. Infrared spectra of the ammonium ion in ammonium hexavanadate  $(\text{NH}_4)_2\text{V}_6\text{O}_{16}$ . *Spectrochim Acta A.* **1990**;46(11):1639–1648.
- [32] Fang Z, Jiao S, Kang Y. Photothermal conversion of  $\text{W18O49}$  with a tunable oxidation state. *Chemistryopen.* **2017**;6(2):261–265.
- [33] Tian Z, Xu Y, Zhu Y. Aldehyde-functionalized dendritic mesoporous silica nanoparticles as potential nanocarriers for pH-responsive protein drug delivery. *Mater Sci Eng C.* **2017**;71:452–459.
- [34] Garcia-Gradilla V, Sattayasamitsathit S, Soto F, et al. Ultrasound-propelled nanoporous gold wire for efficient drug loading and release. *Small.* **2014**;10:4154–4159.